Journal of Achievements in Materials and Manufacturing Engineering
VOLUME 24
ISSUE 1
September
2007

Investigations of causes of dumping conveyor breakdown

E. Rusiński*
co-operating with
J. Czmochowski, P. Moczko
Institute of Machines Design and Operation, Wroclaw University of Technology,
ul. Lukasiewicza 7/9 51-370 Wrocław, Poland
* Corresponding author: E-mail address: eugeniusz.rusinski@pwr.wroc.pl

Received 18.04.2007; published in revised form 01.09.2007

Analysis and modelling

ABSTRACT

Purpose: The main purposes of the paper are to discuss designing and exploitation problems of machines used in strip mines and investigation of its reasons based on steering frame breakdown of the dumping conveyor.
Design/methodology/approach: Numerical (FEM) and experimental approach was used to investigate reasons of the breakdown. Fractographic and microscopic evaluation and chemical analysis, were used to perform material evaluations. The objectives are achieved by analysis of the numerical simulations results and data coming from material evaluations. Additionally the new design of the steering frame was discussed in order to prevent future similar problems in the half-shafts systems.
Findings: The causes of break-down of the steering frame were found. Designing and manufacturing problems were the main reasons of the failure. The undercarriages half shafts systems of the open pit machines are prone to break-downs. They require detailed analysis to be successfully implemented into steering system. Recommendations for the single shaft system are given in the paper.
Research limitations/implications: There are horizontal forces acting on safetying in the half-shaft undercarriage systems, which are limited by the friction in the supporting areas. Investigations of the static and sliding friction coefficients should be performed to estimate correct forces and optimal designing rules.
Practical implications: The study provides practical implication into designing of half-shafts undercarriage systems and their safetyings. Discussed design of the safetying should be redesigned or the half-shaft system should be changed into one shaft design.
Originality/value: The paper provides information backed by evaluation and test results, stating the nexus of causes of the dumping conveyor failure. The experimental and numerical approaches show relationship between designing and manufacturing process of machines. This can be helpful for the designers and researchers looking for reasons, methods of investigations or how to prevent failures of similar machines.
Keywords: CAD/CAM; Constructional design; Materials; Metallography

1. Introduction

The issues relating to damage to and breakdowns and catastrophes of machines and equipment are the subject of numerous researches [18]. If any such event occurs, detailed analyses are carried out to determine its causes, course and results. Thanks to the knowledge gained from such investigations similar cases can be prevented in the future.

The examination of the causes allows one to identify the source of the problem. Moreover, from the user/owner's point of view this may be important in order to file an insurance claim. An analysis of the course of such an event helps to determine its causes and results. A block diagram of interdependencies between the activities involved is shown in fig. 1.

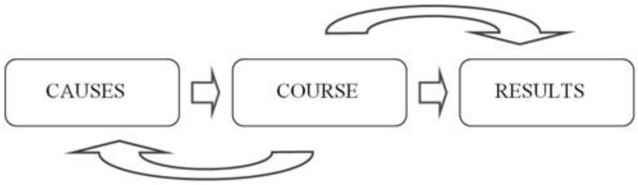

Fig. 1. Interdependencies between causes, course and results of breakdown

To the user the course of a breakdown is not as important as its causes and results while to the researcher it is the course of the breakdown, which is most important since it implies conclusions about both the causes and the results. It is also usually most interesting from researching point of view. This is illustrated below for a breakdown of an overburden dumping conveyor.
In opencast mines, dumping conveyors form a link in the EBD (excavator, belt conveyor, dumping conveyor) system. The operation of a dumping conveyor in a opencast lignite mine [5, 7 and 9] is shown in fig. 2

Fig. 2. Dumping conveyor operating in opencast lignite mine

The overburden which is to be removed from an open pit being mined is transported to dumping conveyor which distributes it on the dump. The dumping conveyor's steerable carriage (fig. 3) broke down during work in winter conditions. The dumping conveyor's driving system consists of one steerable and two nonsteerable caterpillar units. The steerable caterpillar unit is made up of two crawler frames, a carriage and a steering framet. A schematic of the steerable caterpillar unit is shown in fig. 4.

The carriage and the shaft have a box structure made of 25 ÷ 30 mm thick plates. The track girder spacing is 5.9 m and the distance between the steering screw and the track girders' axis is 8.5 m. The investigated dumping conveyor has a system of two axle shafts (halfshafts) joining the track girders to the carriage.

Fig. 3. Breakdown of dumping conveyor's steerable carriage

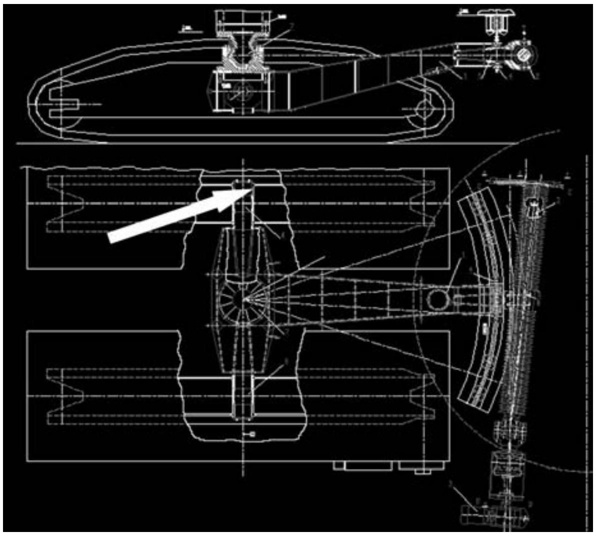

Fig. 4. Schematic of steerable caterpillar unit

This design solution is often used in order to reduce the machine's weight. In such machines the halfshafts are usually 3 m long and have a diameter of 500 mm, decreasing to 300 mm inside the carriage. The resulting mass amounts to about 3.5 tons. This design solution requires, however, solid support and protection against slipping out. The mounting of the halfshaft in the carriage box structure is shown in fig. 5.

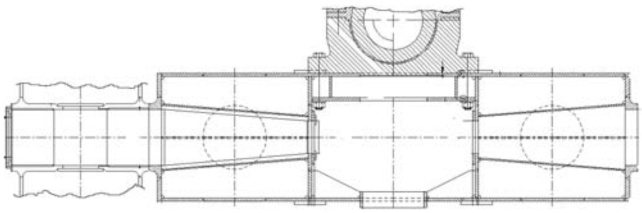

Fig. 5. Halfshaft mounting in carriage structure

The breakdown occurred because one halfshaft slipped out as a result of damage to its slip-out protection. The track girder after the breakdown is shown in fig. 6.

Fig. 6. Breakdown of one carriage: results of steerable carriage breakdown

After the dumping conveyor's gantry together with the machine body had been hoisted and the track girder had been removed the damaged end of the halfshaft could be examined. The halfshaft's damaged end with broken off pieces is shown in fig. 7.

Fig. 7. Damaged halfshaft of steerable carriage

In order to determine the causes of the breakdown the following were carried out:

- an analysis of the forces acting on the steerable unit and on the whole undercarriage in accordance with the current standards [4],
- FEM strength calculations of the steerable unit with the steering shaft,
- defectoscopic tests of the carriage and the halfshafts,
- measurements of carriage plating and halfshaft geometry,
- metallographic examinations of the halfshaft material.

2. Analysis of forces acting on steerable caterpillar unit

The general principles of calculating caterpillar undercarriages can be found in [7] which analyzes in detail the particular travel resistance components, i.e.

- the internal caterpillar track motion resistance,
- the subgrade deformation resistance,
- the climb resistance,
- the curvature travel resistance.

By analyzing the above forces one can determine the loads acting on the particular components of the caterpillar unit. When investigating the causes of the breakdown special attention was paid to the analysis of the forces acting during curvature travel.

According to the current standard for calculating basic surface mining machines DIN 22261-2 [4] calculations should be carried out for the following cases:

- curvature travel (L),
- caterpillar transverse slip (QQ),
- longitudinal dragging (LL), e.g. when the drive of one of the caterpillar tracks fails. In addition one should include the load from the body at a terrain gradient and wind pressure. The protection systems installed on surface mining machinery do not allow one to activate the turn mechanism when the machine does not move. A turn is possible only during travel. The loads acting on the caterpillar unit during curvature travel are shown in fig. 8.

The active forces for the caterpillar unit include:

- body and undercarriage gantry weight V,
- transverse force H produced by lateral forces (due to the terrain gradient and wind pressure),
- the steering force at the end of the shaft, resulting from the friction of the tracks against the ground

$$S = \mu V \frac{i_R}{R_s} \tag{1}$$

where:

μ – the coefficient of caterpillar track friction against the ground (μ = 0.6),

i_R – the radius of gyration of the caterpillar track contact area,

R_s – the distance between the turn mechanism screw axis and the caterpillar track axis.

In FEM calculations [10, 11, 12] one can substitute supports for the active forces (the latter are defined as reactive forces).

The described case of loads analyzed in the FEM calculations played a major role in verifying the choice of bearing element cross sections.

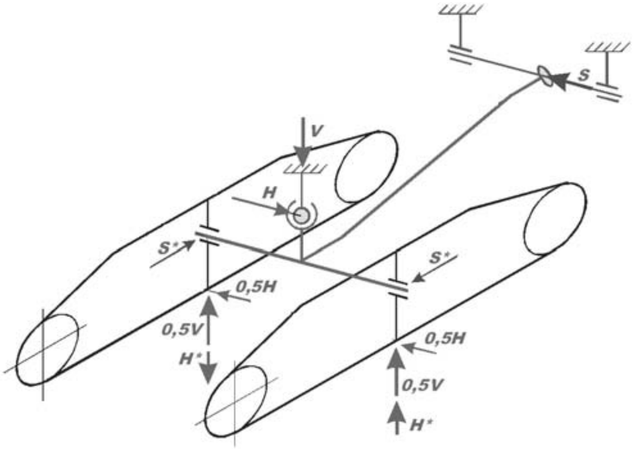

Fig. 8. Forces acting on caterpillar unit during turn

3. FEM strength calculations of caterpillar unit carriage shaft

The caterpillar unit carriage shaft has a box structure. The latter was reproduced using a geometrical model and a discrete shell-beam model. The strength calculations of the caterpillar unit carriage shaft were performed for several cases of loads required by standard [4], using the finite element method [3, 6, 19]. Sample strength calculation results [8] concerning the distribution of the Huber-Misses stress in the steering frame for curvature travel are shown in fig. 9.

Fig. 9. Distribution of Huber - Misses stress in dumping conveyor's steering carriage

For all the required cases of loading no stress levels specified by the standard [1] were found to be exceeded. High stresses were observed only in the vertical ribs of the halfshaft's housing.

4. FEM strength calculations of halfshaft end

The loads acting on the halfshaft, particularly on its end where the slip-out protection is situated, were analyzed. Considerable axial forces produced by the side shearing of soil occur during curvature travel. In unfavourable conditions they and the lateral forces due to the gradient and wind pressure may add up. The protection against halfshaft slip out is shown in fig. 10.

Fig. 10. Halfshaft end - protection against slip out

The plates protecting the halfshaft against slip out were deformed (fig. 11) as a result of the longitudinal movement of the halfshaft .

Fig. 11. Deformed elements (plates) protecting against halfshaft slip out

Due to the axial clearance of the halfshaft static friction μ = 0.09-0.14 becomes sliding friction μ = 0.01-0.05. One should note that in this case sliding friction should not occur, but it did occur as evidenced by the deformation of the protective plates (fig. 11). FEM calculations of the halfshaft end were carried out for the most unfavourable case of loading. One should note that because of the very small rounding radius at the bottom of the groove for the protective plates considerable stress concentrations arise under the action of axial forces. The radius is as small as r = 0.2 mm (as measured on microsections of the protection). The halfshafts were made of toughened constructional alloy steel 42CrMoS4 whose yield point is Re = 880 N/mm2 and strength Rm = 1030 N/mm2. The FEM strength calculations of the halfshaft were performed for two values of the axial force acting on the halfshaft protection:

- axial force F = 1393 kN – the axial force at travelling along a curvature with radius R = 60 m with the terrain gradient and wind pressure (HZS (L)) taken into account and with neglected friction ($\mu = 0$) on the halfshaft mounting hubs,
- axial force F = 704 kN – the axial force at travelling along a curvature with radius R = 60 m with terrain gradient and wind pressure (HZS (L)) and friction ($\mu = 0.09$) on the halfshaft mounting hubs taken into account.

The first case is rather theoretical since it assumes that total axial force F = 1393 kN acts on the halfshaft's end. But some of the axial force is taken by friction between the hub and the journal at the places of halfshaft mounting. According to standard [4] the coefficient of friction in this case can be assumed at a level of μ = 0.09-0.22. Assuming the less favourable friction coefficient value ($\mu = 0.09$) and knowing the forces in the bearings, the axial force taken by the halfshaft's end was determined to be F = 704 kN. Figure 12 shows the distribution of Huber-Mises stress determined by FEM calculations [8] for radius r = 0.2 mm and r = 4 mm while the maximum Huber-Mises stresses on the groove's bottom for two values of the axial force transmitted by the halfshaft lug are given in table 1. The rounding radius of 4 mm was adopted for comparison purposes in order to determine its safe (strength wise) value.

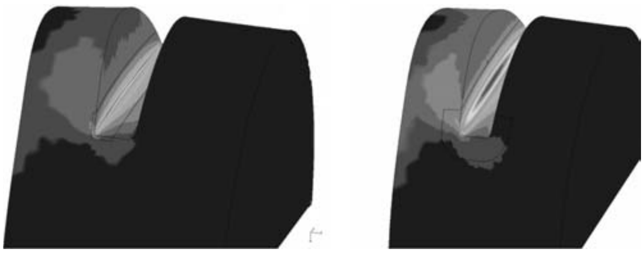

Fig. 12. Distribution of Huber-Mises reduced stress in slide-out protection groove (nonlinear elastoplastic calculations): a) r = 0.2 mm, b) r = 4 mm

Table 1.
Maximum Huber-Mises stresses in analyzed halfshaft end

Calculations	Axial force F [kN]	Rounding radius r [mm]	Reduced stress σ [MPa]	Safety factor δ
without friction	1393	4	822	1.07
		0.2	1080 (1780*))	0.49
with friction	704	4	405	2.17
		0.2	880	1.00

*) a theoretical value for material elasticity in the full load range.

The FEM [20] calculations indicate that at the bottom of the groove with radius r = 0.2 mm stresses considerably exceed the yield point. The stresses come down below the yield point at radius r = 4 mm.

5. Metallographic examination of halfshaft

Metallographic examinations were carried on three elements from the fractured caterpillar halfshaft. The elements were denoted as 1, 2 and 3 (figs 13 and 14). Naked-eye macroscopic examinations and examinations by means of a stereoscopic microscope at a magnification of 30x were conducted. Also microscopic examinations using a NEOPHOT 32 light microscope and a digital camera were performed.

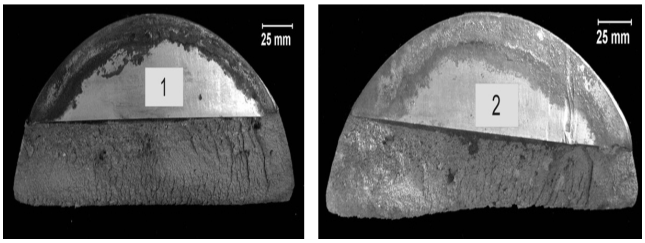

Fig. 13. Fragments broken off caterpillar halfshaft – element 1 and 2

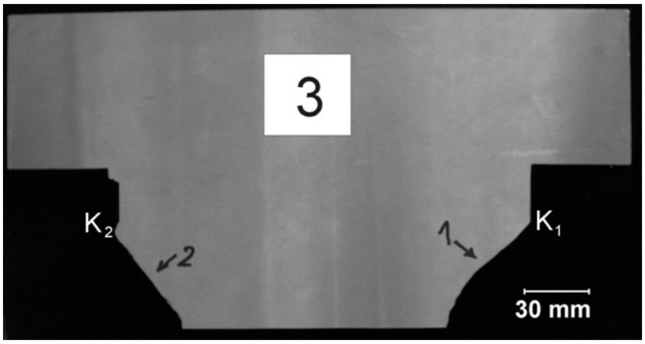

Fig. 14. Piece cut out from damaged halfshaft cross section – element 3

The macroscopic examinations showed fractures originating in the caterpillar half-shaft. The fractographic investigations showed that the fractures had fatigue fracture features, including a temporary coarse-grained brittle zone (figs 15 and 16). In element 1 the fatigue zone area is located near edge AC and it takes up about 2% of the fracture area. The fatigue zone area in element 2 is located near edge EG, occupying about 4% of the fracture area (fig. 14). The fractures were locally coated with corrosion products. The fatigue zones have a lenticular shape, most wide close to the middle of edges AC and EG in the investigated elements [13 and 17]. The places are denoted as S1 and S2 for respectively elements 1 and 2. The fatigue zone in point S1 is about 3 mm wide against the temporary zone width of about 65 mm while in point S2 it is about 6 mm wide against the temporary zone width of about 60 mm (fig. 15). In the case of element 1, the first fatigue zone area is located by edge A and the second one at a distance of about 20 mm from edge C. Similarly in element 2 one fracture fatigue zone area is located directly at edge E while the other at a distance of about 10 mm from edge G. Such a fatigue fracture structure indicates that the largest stresses occur in the medial part of the groove towards points A and C (element 1) and E and G (element 2).

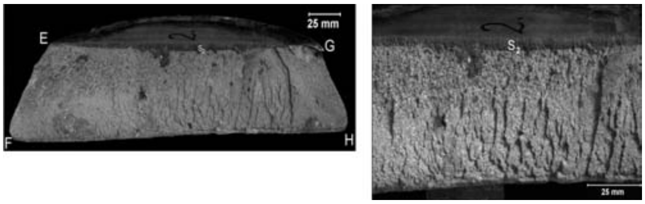

Fig. 15. General view of surface of fracture with marked edges. Symbol S2 marks widest fracture fatigue zone area

It was found that both fractures had been initiated at the place where the cross section changes. The fatigue zone is located along the undercuts denoted by symbols K1 and K2 in fig. 14. The fracture of element 1 ran parallel to edge AC and at an angle of 45 deg. to the halfshaft's longitudinal symmetry axis by edge GH. The angle gradually increases to-wards edge EF, reaching 60 deg.. This indicates that in element 1 the fracture of the half-shaft groove resulted from the action of shearing forces and bending moments on it. As a result of damage to element 1 an additional bending moment was produced (as one point of support was removed) whereby the direction of fracture propagation changed in element 2, as evidenced by the clear plastic deformation in point G, which probably occurred in the final stage of fracturing (fig. 16).

Fig. 16. Element 2. Magnified fragment from fig. 15(visible plastic deformation in point G)

The small area of the fatigue zone in comparison with that of the temporary zone is evidence of great strain of the halfshaft material. This means that either too low safety factors were adopted or the allowable stress was considerably exceeded during operation. Also improper heat treatment of the element's structural material could be the cause. The most likely places of fracture initiation are points A and C (element 1) and E and G (element 2) where a local stress concentration might have occurred because of the change in the cross section. The fact that the fracture occurred in the middle section of edges AC and EG may suggest either nonuniform distribution of stresses (surface pres-sures) in the groove or a manufacturing or structural notch. The nonuniform stress pattern in the halfshaft groove could also be due to the faulty fabrication of the grooves, and also of the plates (e.g. their clamping surfaces not being flat and parallel). The signs of wear on the clamping surfaces indicate that the surface pressures were distributed on the groove's circumference and not over its whole surface. This distribution of clamping stresses explains the lenticular shape of the fatigue zone: since the clamping forces are uniformly distributed on the circumference, the maximum bending moments produced by them occurred in the groove's middle part in the region of points S1 and S2. The place from which the specimens were taken is shown in fig. 17.

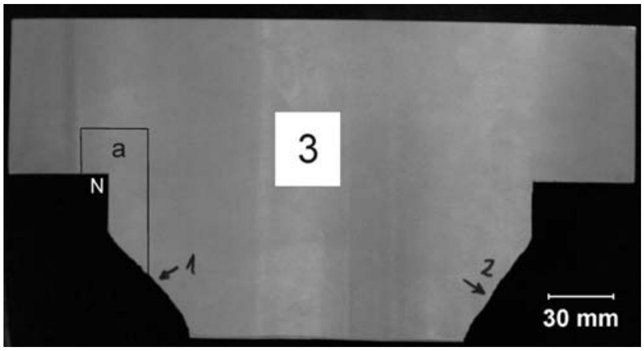

Fig. 17. Place (determined by macroscopic examinations) where specimens for further metallographic studies were taken

On both sides of specimen a the radius on the edge of the halfshaft groove for sliding in the protective plates was measured in the place marked N in fig. 17. A transition with curvature radius r=0.2 mm was found. This radius is too small to be a manufacturing radius.

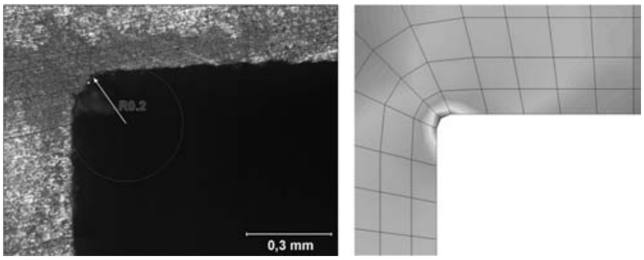

Fig. 18. Location of halfshaft groove; a) groove edge curvature radius r = 0.2 mm on specimen's left side, b) plastic strain zone on groove's bottom

Microscopic examinations were carried out on unetched and etched (with Mi1Fe re-agents) microsections. The results of the examinations are shown as microphotographs in figs 19-22.

In the unetched microsections non-metallic inclusions, mainly in the form of sulphides uniformly distributed over the whole surface of the specimen along the direction of plastic forming (fig. 19), were found.

After etching with Mi1Fe a pearlitic-ferritic structure (locally in the form of the Widmanstätten structure) was observed (fig 21). Such a microstructure is the result of local inhomogeneity in chemical composition, caused by improper heat treatment and plastic forming and incomplete reforging of the steel because of the considerable thickness of the component. Consequently, the material's mechanical properties might have deteriorated [16].

The examinations also showed a crack originating from the groove's edge, running parallel to the cross section change edge at an angle of 45deg to the shaft's axis and running along the boundaries of ferrite and pearlite grains (fig. 22).

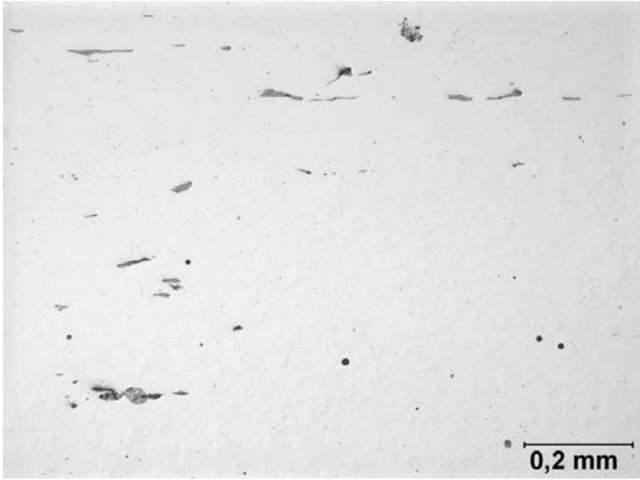

Fig. 19. Non-metallic inclusions uniformly distributed over whole surface of micro-section along direction of plastic working. Unetched condition. Light microscopy

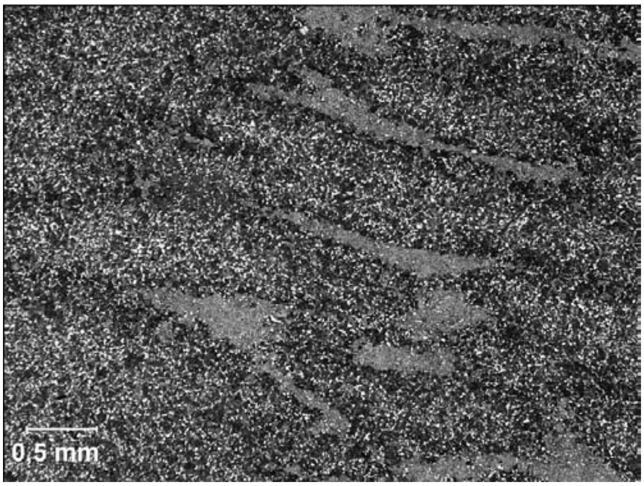

Fig. 20. Inhomogeneous pearlitic-ferritic structure. Etched condition. Light micros-copy

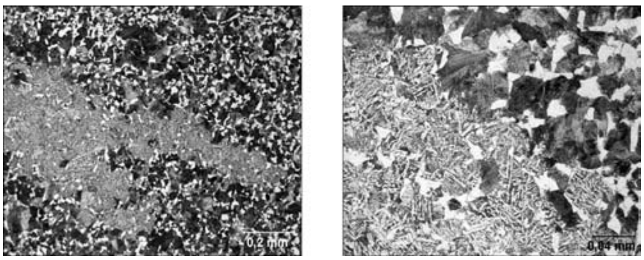

Fig. 21. Etched condition. Light microscopy: a) inhomogeneous pearlitic-ferritic mi-crostructure with features of Widmanstätten structure, b) magnified fragment

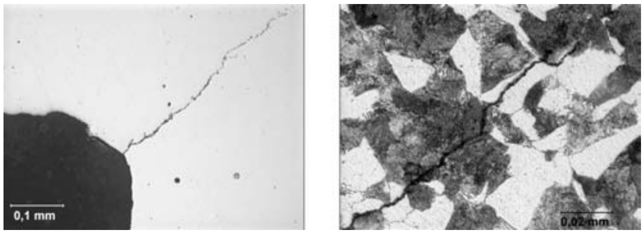

Fig. 22. Edge of lock groove. Light microscopy: a) visible crack initiated in area where cross section changes – unetched condition, b) magnified fragment of area in etched condition, visible crack running along boundaries of ferrite and pearlite grains

6. Conclusions

The FEM analyses of the caterpillar unit and of the halfshaft end showed that the main cause of the breakdown was the way in which the halfshaft had been protected against slipping out. The fractures in the caterpillar support halfshaft lock are of the fatigue type: the temporary part is brittle and coarse-grained. The fatigue zones were initiated at the place where the cross section changes. They extend from the groove's edge into the material at an angle of about 45deg to the halfshaft's symmetry axis and have a lenticular shape which is widest near the middle of the groove's edge. The fatigue zone area in specimen 1 amounts to 2% and in specimen 2 to about 4%. This fatigue fracture structure suggests that the largest stresses occurred in the groove's medial part.

Because of the low ratio of fatigue zone area to temporary zone area a considerable effort of the structure or the adoption of very low safety factors could have been the case. The investigated element has a pearlitic-ferritic structure with locally occurring Widmanstätten structure features which might have resulted in the deterioration of the material's mechanical properties. Such a structure indicates that the element was not properly heat treated. Microscopic examinations of element 3 revealed the presence of cracks (fig. 21) indicating the onset of fatigue fracture. The cracks were initi-ated at the place at the groove's bottom where the cross section changes and they ex-tend into the material at angle of about 45deg parallel to the whole edge of the speci-men taken from the element. The examinations showed that the slip-out protection had not been properly designed and made. The direct cause of the breakdown was the too small rounding radius of the groove's bottom (r = 0.2), leading to fracture, sliding out of the halfshaft and the breakdown of the dumping conveyor. A fatigue analysis of the groove's bottom showed that the halfshaft material was in the range of limited fatigue strength (fig. 23). Hence it is concluded that the adopted protection is not good for this system of fixing the halfshafts. A much better solution is an annular protection with a properly large rounding radius of the halfshaft groove. The undercarriage system consisting of two halfshafts is advantageous from the fabrication and weight points of view. An alternative could be a single-shaft design in which the slide-out protection is much simpler (vertical protection in the form of an additional shaft). But this system would be much heavier (hollow shafts could be employed to reduce the weight) and more expensive.

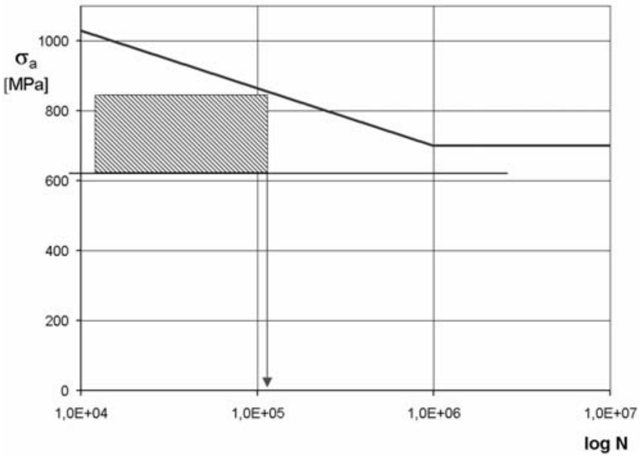

Fig. 23. Wöhler diagram for steel 40HM with marked limited fatigue strength region for radius r = 0.2 mm in halfshaft grooves

Since many breakdowns of two-shaft undercarriages have been reported it can be concluded that such systems require more care in their design as compared with single-shaft systems. It can be helpful here to run numerical simulations to identify the weak points of the design. This approach was adopted in the present research. Also friction forces at the places where the halfshafts are supported play a significant role. Depending on the kind of friction (static or sliding) they can reach different magnitudes. In many cases, such loads determine the safety of operation of the undercarriage. But the magnitudes of the forces have not been precisely identified yet. Therefore further experimental re-search is needed to make the design of such systems more accurate.

References

[1] J. Brändlein, Elastische Verformungen der Gehäuse beeinflussen die Wälzlagerung. Maschienenmarkt 56 (1980).

[2] Ch.R. Brooks, A. Choudhury, Failure analysis of engineering materials. New York, McGraw-Hill, 2002.

[3] R.D. Cook, D.S. Malkus, M.E. Plesha, R.J. Witt, Concepts and Applications of Finite Element Analysis, 4th Edition, John Willey, New York, 2001.

[4] DIN/22261-2 – Bagger Absetzer und Zusatzgeräte in Braunkohlentagebauen, Teil 2: Berechnungsgrundlagen.

[5] D. Dudek, KRUPP-Schaufelradbagger SchRs-4600 in polnischen Tagebauen. Braunk. Tagebautech 38 H 1/2, 1986.

[6] J.M. Dulieu-Barton, M.J. Brennan, Damage assessment of structures, Proceedings of the 5th International Conference on Damage Assessment of Structures DAMAS 2003, Southampton, UK, 2003.

[7] W. Durst, W. Vogt, Schaufelradbagger. Trans Tech Publications, 1986.

[8] I-DEAS Master Series, Mechanical CAE/CAD/CAM Software, Structural Dynam-ics Research Corporation, 2000 Eastman Dr., Milford, OH 45150

[9] H. Hawrylak, R. Sobolski, Open cast mining machines. Publisher „Śląsk”, Katowice 1967.

[10] E. Rusiński, J. Czmochowski, T. Smolnicki, Advanced Finite Element Method for Load-carrying Structures of Machines, PWN, Wroclaw, 2000 (in Polish).

[11] E. Rusiński. Finite Element Method; System COSMOS/M, WKŁ, Warsaw, 1994 (in Polish).

[12] O.C. Zienkiewicz, R.L. Taylor, The Finite Element Method, Solid Mechanics 5th edition, Butterworth-Heinemann, 2000.

[13] J. Schijve, Fatigue of structures and materials, Dordrecht, Kluwer Aca-demic, 2001.

[14] B. Schlecht, Modern Drive Technology for the Mining and Minerals Industry. Bulk Solids Handling in Surface Mines, Trans Tech Publications, Clausthal-Zellerfeld, 2000.

[15] B. Schlecht, Effektive Überlastsicherung in Schaufelradantrieben. Braunkohle 50 (1998).

[16] C.W. Wegst, Stahlschlüssel. Verlag Stahlschlüssel Wegst, Marbach, 2001

[17] B. Wurm, Ermüdungsuntersuchungen an scharf gekerbten Proben. Zugl.: Dresden, Techn. Univ., Diss., 1999 Düsseldorf : VDI-Verl., 2000

[18] E. Rusinski, J. Czmochowski, P. Moczko, Numerical and experimental analysis of a mine’s loader boom crack, Journal of Achievements in Materials and Manufacturing Engineering 17 (2006) 273-276.

[19] Y. Zhang, D. Redekop, Shell element simulation of the push method of tube bending, Journal of Achievements in Materials and Manufacturing Engineering 17 (2006) 301-304.

[20] E. Rusinski, A. Kopczynski, J. Czmochowski, Tests of thin-walled beams joined by spot welding, Journal of Materials Processing Technology 157-158 (2004) 405-409.